ChemComm

COMMUNICATION

View Article Online
View Journal | View Issue

Cite this: *Chem. Commun.*, 2025, **61**, 4971

Received 30th December 2024,
Accepted 27th February 2025

DOI: 10.1039/d4cc06804a

rsc.li/chemcomm

Combining broadband absorbing electrochromic materials for hybrid grey-to-colourless flexible devices†

Lukas Niklaus, ‡[a] Rúben R. Ferreira, ‡[b] Sven Macher, [a] Antoine Stopin, [b] Marco Schott, *[a] Laura Maggini *[b] and Davide Bonifazi [b]

This study presents a grey-to-colourless hybrid electrochromic device combining a novel red-to-colourless polymer with blue-to-colourless Prussian blue. The device achieves a neutral tint in both the dark and bleached states, with notable changes in visible light transmittance and fast response.

Electrochromic materials (ECMs) and devices (ECDs) exhibit a colour change upon the application of an electrical stimulus.[1] This colour change is caused by variations in the oxidation state of ECMs, accompanied by the insertion or extraction of ions into the ECM layer to balance the charge. ECMs can be classified as inorganic[2–5] (*e.g.*, metal oxides), organic[6–8] (*e.g.*, conjugated polymers), or hybrid inorganic–organic[9–11] (*e.g.*, metallo-polymers). Among these, electrochromic conjugated polymers (ECPs) have attracted considerable interest due to their high optical contrast and colouration efficiency, fast response, and broad colour range[12–17] achievable through structural design. As a result, ECP-based ECDs have found applications in diverse fields, including smart windows,[8] colour-changing fabrics,[7] and adaptive camouflage.[18,19] Interest in neutral-tint ECDs has increased due to their potential application in light-dimmable systems, eyewear, automobiles, and architecture, where black/grey-to-colourless transitions with minimal colour distortion are desirable.[20,21] Although donor–acceptor (DA) ECPs are commonly used to obtain these transitions,[22–24] they suffer from residual colour in the bleached state.[25] Additionally, their complex synthesis, challenges with large-scale production, and cost hinder practical application.

An alternative approach involves combining two or more ECMs with complementary colours, achieving neutral hues through subtractive colour mixing.[26,27] The careful selection of complementary ECMs can optimise the final hue by broadening the light absorption across the visible spectrum, resulting in a perceived neutral colouration.[12,28–30] For instance, Sotzing *et al.* demonstrated colour neutrality achieved by subtractive colour mixing of either blue PEDOT[31] or purple PProDOT electropolymerised *in situ* in combination with a yellow organic dye in the electrolyte.[32] To eliminate potential issues related to the *in situ* polymerisation of complex ECMs, an alternative could involve the controlled deposition of the complementary ECMs onto separate electrodes. In this arrangement, the secondary ECM can serve as both a hue regulator for the primary ECM and a charge-balancing layer,[33] simplifying ECD assembly. Complementary ECMs with opposing redox behaviours can create the desired subtractive colour mixing effect, ensuring that the display alternates between coloured and colourless states when an electrical potential or current is applied.

In this work, we present a hybrid grey-to-colourless switching ECD that combines a novel organic ECP (**Red1**), which transitions from red to colourless, with Prussian blue (**PB**), an inorganic material known for its reversible blue-to-colourless transition (Fig. 1). While **Red1** bleaches upon oxidation, **PB** bleaches upon the reduction of $[Fe(III)CN_6]^{3-}$ to $[Fe(II)CN_6]^{4-}$.[34,35] This pairing leverages broadband absorption in the visible range (400–800 nm), with complementary redox behaviour, making it highly effective for neutral-tint ECDs while maintaining scalability and assembly simplicity.

Achieving a fully red-to-colourless, fast-switching ECP is a challenging task, as the high bandgap needed to produce a red colour makes it difficult to shift the bipolaronic transition to the NIR after oxidation.[36–39] Reynolds and coworkers tackled this task by developing a 1 : 1 copolymer of an electron-rich bulky acyclic dioxythiophene (3,4-di(2-ethylhexyloxy)thiophene; DEHOT), with smaller monomers (3,4-di(methoxy)thiophene; DMOT).[36] The electron-donating oxygenated substituents on the thiophene ring lower the oxidation potential and enable a transmissive oxidised state by stabilising a closed-shell bipolaron structure.[40]

[a] *Fraunhofer Institute for Silicate Research ISC, Neunerplatz 2, D-97082 Würzburg, Germany. E-mail: marco.schott@isc.fraunhofer.de*
[b] *Department of Organic Chemistry, University of Vienna, Währinger Straße 38, A-1090 Vienna, Austria. E-mail: laura.maggini@univie.ac.at*

† Electronic supplementary information (ESI) available. See DOI: https://doi.org/10.1039/d4cc06804a

‡ These authors contributed equally to this work.

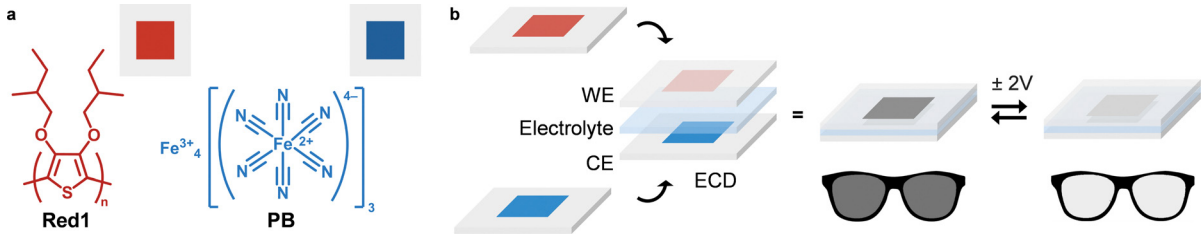

Fig. 1 (a) Structures of **Red1** and **PB**; (b) schematic representation of the assembly of electrodes to provide a neutral-tint ECD and potential application in eyewear. WE = working electrode (**Red1**), CE = counter electrode (**PB**).

The branched alkyl groups enhance solubility and introduce steric effects that reduce the conjugation length. Additionally, these groups create an "open" morphology that facilitates ion transport through the film.[36,37] However, the 2-ethylhexyl chains alone would introduce excessive steric repulsion in the ECP, resulting in an orange colour and slow response. Smaller monomers are needed to lower the band gap further and achieve a red hue. Additionally, side-chain entanglement can reduce interchain spacing, impeding rapid ion transport.

To address these issues and facilitate scalable synthesis for industrial applications, we designed a dioxythiophene monomer, 3,4-di(2-methylbutyloxy)thiophene (DMBOT; **1**), that can polymerise into a red-coloured ECP (**Red1**; Fig. 1a) exhibiting a rapid red-to-colourless transition. The branched 2-methylbutyl side chain provides sufficient steric bulkiness to reduce conjugation length for the red hue while maintaining a transparent oxidised state and an open morphology to support efficient ion intercalation and fast switching.

Monomer **1** was synthesised according to published procedures,[41] before undergoing ferric chloride ($FeCl_3$) catalysed oxidative polymerisation[42] to produce **Red1** (see ESI†). Initially, a **Red1**/**Red1** ECD with an active area of 1 cm^2 was prepared to characterise the ECP (Fig. 2). Spectroelectrochemical analysis revealed the desired broad transmittance minimum centred at 500 nm (Fig. 2a), responsible for the red colour. Upon applying different cell voltages (±1.5 V), the absorbance of the ECD shifted bathochromically into the NIR region, with a clear isosbestic point observed at 610 nm (Fig. S6, ESI†). This behaviour is characteristic of polythiophenes[26,43] and is attributed to the increased conjugation along the polymer backbone due to the formation of bipolarons during oxidation. The visible light transmittance (VLT, τ_v) of the dark (37%) and bleached (61%) state corresponds to a total modulation ($\Delta\tau_v$) of 24%. The colour of the ECD was assessed using the CIELAB system, as described in DIN 5033.[44] This ECD presented a significant increase in the a^* value from the bleached (a^* = −2.2) to the dark (a^* = 27.9) state, indicative of its red colour. Switching times for both bleaching and colouring processes were evaluated using chronoamperometry while recording the voltage-induced colour change in transmittance at 500 nm (Fig. 2b). The switching time is defined as the time required to achieve 90% of the total transmittance change, in a given timeframe. The determined values at ± 1.5 V were 1.8 s for colouring and 3.8 s for bleaching, highlighting how **Red1** can achieve a high optical contrast with fast switching.

After evaluating the EC properties of **Red1**, we investigated its combination with **PB** counter electrodes presenting different thicknesses (**PB1**, **PB2**, and **PB3**) to achieve a neutral-tint ECD (Fig. 3a and b). **PB** thin-film electrodes were prepared on ITO-coated PET substrates (see ESI†), and their transmittance spectra were measured (Fig. 3a). The light blue **PB** films exhibited a broad intervalence charge transfer (IVCT) band centred around 700 nm, characteristic of mixed-valence compounds.[45] By adding the absorbance of the **PB** films to that of **Red1**, the predicted transmittance of the resulting ECDs was calculated (Fig. 3b). Based on these calculations, we determined the $L^*a^*b^*$ values for the various electrode combinations (Table S2, ESI†). Among these, the ECD using **PB2** as counter electrode is expected to achieve the lowest a^* and b^* colour coordinates, indicating a near-neutral tint. Based on these results, we evaluated the

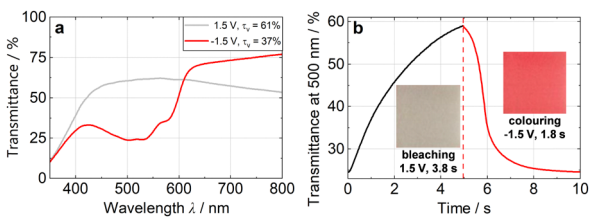

Fig. 2 (a) Spectroelectrochemical characterization and (b) switching time determination of the **Red1**/**Red1** ECD at cell voltage ± 1.5 V.

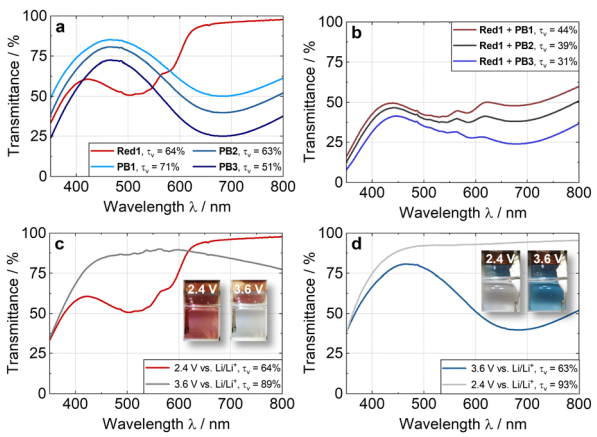

Fig. 3 (a) UV-vis absorbance spectra of three different **PB** electrodes and (b) their combination with **Red1**; spectroelectrochemical characterization of the (c) **Red1** and (d) **PB2** electrodes with Li as CE/RE in 1 M LiTFSI/PC.

individual EC performance of the **Red1** and **PB2** electrodes in an electrochemical half-cell with Li as the counter electrode (CE) and reference electrode (RE), using 1 M lithium bis(trifluoromethane)-sulfonimide (LiTFSI) in propylene carbonate (PC) as the electrolyte (Fig. 3c and d). For **Red1**, the broad transmittance band (λ_{max} = 504 nm) increased upon oxidation at 3.6 V *vs.* Li/Li^+ and reduced upon reduction at 2.4 V *vs.* Li/Li^+ (cathodically colouring, Fig. 3c), while **PB2** exhibited a colour change between 2.4 V and 3.6 V *vs.* Li/Li^+ (anodically colouring), observable by the broad IVCT transition at around 685 nm after oxidation (Fig. 3d).

The τ_v value [dark/bleached in %] changed between 63/89 and 63/93 for **Red1** and **PB2**, respectively (Table 1). Notably, both electrodes reached an almost completely colourless bleached state, with a^*/b^* values of −1.0/3.6 for **Red1** and −0.9/−3.1 for **PB2**. Additionally, both electrodes were analysed using cyclic voltammetry (CV), charging/discharging, and cycle stability measurements over 1000 switching cycles. **Red1** exhibited anodic and cathodic peak potentials, E_{pa} and E_{pc}, corresponding to the oxidation (bleaching) and reduction (colouring) processes at 3.36 V and 3.51 V *vs.* Li/Li^+, respectively, at a scan rate of 10 mV s^{-1} (Fig. S8, ESI†). For **PB2**, the anodic and cathodic peak potentials appeared at 2.78 V and 3.04 V *vs.* Li/Li^+ (Fig. S8, ESI†). No side reactions were observed within the applied potential window (2.4–3.6 V).

Charge densities determined by galvanostatic measurements (Fig. S9, ESI†) revealed a maximum charge density of 0.62 mC cm^{-2} for **Red1** and 4.87 mC cm^{-2} for **PB2** at a current density of 1 μA cm^{-2}. Another key performance indicator for ECMs is the colouration efficiency (η), which is calculated using the equation: $\eta = \log(T_b/T_d)/q$, where T_b and T_d are the transmittance values in the bleached and dark states, respectively, and q is the charge density. The η values for **Red1** and **PB2** were determined to be 359 cm^2 C^{-1} (at 504 nm) and 78 cm^2 C^{-1} (at 685 nm), respectively. The CV (Fig. S8, ESI†) and charge/discharge measurements of the **Red1** electrodes confirmed the high reversibility of the bleaching and colouring processes (Fig. 4a). At a current density of 50 μA cm^{-2}, the Coulombic efficiency (defined as the ratio of discharge to charge density) exceeded 92%. Cycling tests of the individual electrodes in inert conditions (see ESI†) revealed that after 1000 charge/discharge cycles between 2.4 V and 3.6 V *vs.* Li/Li^+, the **Red1** electrode retained over 84% of its initial charge (0.67 mC cm^{-2} → 0.56 mC cm^{-2}). A similar evaluation of the **PB2** electrode showed a Coulombic efficiency above 97% (Fig. 4b), with charge retention over 88% (4.69 mC cm^{-2} → 4.13 mC cm^{-2}), indicating stable redox behaviour.

Finally, the **Red1** and **PB2** electrodes were assembled into a grey-to-colourless ECD (**Red1**/**PB2**) with an active area of 5 × 5 cm^2.

Table 1 $L^*a^*b^*$ colour coordinates, visible light transmittance (τ_v), and colouration efficiency (η) of the **Red1** and **PB2** EC electrodes

EC electrodes	Potential/V *vs.* Li/Li^+	L^*	a^*	b^*	τ_v/%	$\Delta\tau_v$/%	η/cm^2 C^{-1}
Red1	2.4	83.0	17.7	4.8	63	26	359
	3.6	95.3	−1.0	3.6	89		
PB2	2.4	97.0	−0.9	3.1	93	30	78
	3.6	84.7	−12.8	−10.3	63		

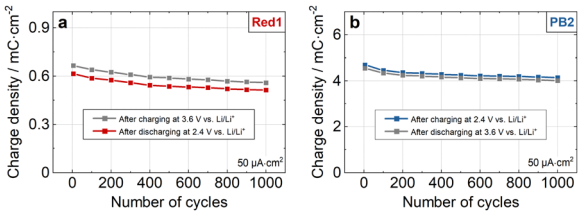

Fig. 4 Charge/discharge measurements over 1000 switching cycles for (a) **Red1** and (b) **PB2**, performed at 50 μA cm^2.

The device was fabricated using a sheet-to-sheet assembly process (see ESI†), using a proprietary LiTFSI-containing gel electrolyte.[46] Spectroelectrochemical analysis of the device revealed that in its dark state, a grey colour can be achieved at a cell voltage of −2.0 V (Fig. 5). This grey hue results from the **PB2** counter electrode absorbing in the 600–800 nm region, which perfectly complements the lower wavelength absorption (400–600 nm) of the cathodically colouring **Red1** (Fig. 5a). The measured colour coordinates of the dark (a^*/b^* = −5.3/−4.7) and bleached state (a^*/b^* = −3.2/−0.5) closely match the calculated values and confirm the neutral colouration. The ECD could be reversibly switched to a colourless state at 2.0 V, with τ_v values of 29% in the dark state and 63% in the bleached state. The switching time of the ECD, determined from the τ_v-time profile shown in Fig. 5b, was around 11 s for bleaching and 9 s for colouring, highlighting the device's suitability for EC applications requiring fast response. The relevant optical properties and switching times are summarised in Table 2. Further characterization by CV (Fig. S10, ESI†), showed well-defined, reversible redox peaks at cell voltages of approximately 0.76 V (bleaching) and 0.55 V (colouring) at a scan rate of 10 mV s^{-1}. Moreover, the scan-rate-dependent CVs (10–100 mV s^{-1}) indicate that the oxidative and reductive peak currents are linearly proportional to the square root of the scan rate, *i.e.* the bleaching/colouring processes are diffusion-controlled.

In summary, we developed a simple and scalable method for producing grey-to-colourless switching ECDs. A novel red ECP (**Red1**) was designed and straightforwardly synthesised,

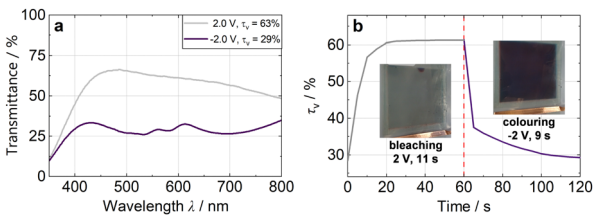

Fig. 5 (a) Spectroelectrochemical characterization and (b) switching time determination of the **Red1**/**PB2** ECD at cell voltage ± 2 V.

Table 2 $L^*a^*b^*$ colour coordinates, visible light transmittance, and switching time of the **Red1**/**PB2** ECD

Full Cell	Cell voltage/V	L^*	a^*	b^*	τ_v/%	$\Delta\tau_v$/%	Switching time/s
Red1/**PB2**	2.0	83.6	−3.2	−0.5	29	34	11
	−2.0	61.7	−5.3	−4.7	63		9

presenting a fast red-to-colourless transition and cycling resilience within flexible ECDs. By combining **Red1** with **PB** for complementary switching, we achieved a hybrid grey-to-colourless switching ECD with a VLT modulation of 34% and switching times of approximately 10 s (active area 5 × 5 cm^2). This approach shifts grey-to-colourless ECD development from synthetic challenges to an assembly-focused strategy, enhancing the potential of electrochromic technology for cost-effective applications.

This work was supported by the European Union's Horizon 2020 research and innovation program (grant no. 760973, DecoChrom). DB, LM and RF further acknowledge the University of Vienna for funding and Dong Min Lee and Dr Sayan Sarkar for the NMR, HRMS and GPC analysis of 1 and Red1 polymer. The authors would also like to thank Christine Müller for the preparation of the PB electrodes and hybrid ECDs.

Data availability

The data supporting this article have been included in the ESI.†

Conflicts of interest

There are no conflicts to declare.

Notes and references

1 *Electrochromic materials and devices*, ed. D. R. Rosseinsky, P. M. S. Montk and R. J. Mortimer, Wiley-VCH, Weinheim, 2015.
2 G. A. Niklasson and C. G. Granqvist, *J. Mater. Chem.*, 2007, **17**, 127–156.
3 L. Niklaus, M. Schott, U. Posset and G. A. Giffin, *ChemElectroChem*, 2020, **7**, 3274–3283.
4 A. Paolella, C. Faure, V. Timoshevskii, S. Marras, G. Bertoni, A. Guerfi, A. Vijh, M. Armand and K. Zaghib, *J. Mater. Chem. A*, 2017, **5**, 18919–18932.
5 C. G. Granqvist, *Thin Solid Films*, 2014, **564**, 1–38.
6 K. Madasamy, D. Velayutham, V. Suryanarayanan, M. Kathiresan and K.-C. Ho, *J. Mater. Chem. C*, 2019, **7**, 4622–4637.
7 W. M. Kline, R. G. Lorenzini and G. A. Sotzing, *Color. Technol.*, 2014, **130**, 73–80.
8 R. J. Mortimer, A. L. Dyer and J. R. Reynolds, *Displays*, 2006, **27**, 2–18.
9 L. Niklaus, M. Schott, M. Mihelčič, I. Jerman, U. Posset and G. Sextl, *Sol. Energy Mater. Sol. Cells*, 2019, **200**, 110002.
10 M. Schott, H. Lorrmann, W. Szczerba, M. Beck and D. G. Kurth, *Sol. Energy Mater. Sol. Cells*, 2014, **126**, 68–73.
11 M. Schott, L. Niklaus, J. Clade and U. Posset, *Sol. Energy Mater. Sol. Cells*, 2019, **200**, 110001.
12 R. H. Bulloch, J. A. Kerszulis, A. L. Dyer and J. R. Reynolds, *ACS Appl. Mater. Interfaces*, 2015, **7**, 1406–1412.
13 J. A. Kerszulis, K. E. Johnson, M. Kuepfert, D. Khoshabo, A. L. Dyer and J. R. Reynolds, *J. Mater. Chem. C*, 2015, **3**, 3211–3218.
14 P. M. Beaujuge, S. Ellinger and J. R. Reynolds, *Adv. Mater.*, 2008, **20**, 2772–2776.
15 A. Cihaner and F. Algı, *Adv. Funct. Mater.*, 2008, **18**, 3583–3589.
16 L. You, J. He and J. Mei, *Polym. Chem.*, 2018, **9**, 5262–5267.
17 M. Schott, L. Niklaus, S. Janietz, C. Völkel, T. Egorov-Brening and T. Bilkay-Troni, *Polymers*, 2024, **16**, 799.
18 H. Fu, L. Zhang, Y. Dong, C. Zhang and W. Li, *Mater. Chem. Front.*, 2023, **7**, 2337–2358.
19 J. Wang, L. Zhang, W. Zhan, J. Dong, Y. Ma, J. Li, W. Li and C. Zhang, *Chem. Eng. J.*, 2024, **483**, 149078.
20 M. Sassi, M. M. Salamone, R. Ruffo, G. E. Patriarca, C. M. Mari, G. A. Pagani, U. Posset and L. Beverina, *Adv. Funct. Mater.*, 2016, **26**, 5240–5246.
21 V. Rai, R. S. Singh, D. J. Blackwood and D. Zhili, *Adv. Eng. Mater.*, 2020, **22**, 2000082.
22 G. Sonmez, C. K. F. Shen, Y. Rubin and F. Wudl, *Angew. Chem.*, 2004, **116**, 1524–1528.
23 S. Ozdemir, M. Sendur, G. Oktem, Ö. Doğan and L. Toppare, *J. Mater. Chem.*, 2012, **22**, 4687.
24 H. Yue, S. Ming, H. Du, J. Zhao and Y. Zhang, *Eur. Polym. J.*, 2022, **175**, 111395.
25 A. M. Österholm, L. Nhon, D. E. Shen, A. M. Dejneka, A. L. Tomlinson and J. R. Reynolds, *Mater. Horiz.*, 2022, **9**, 252–260.
26 P. M. Beaujuge and J. R. Reynolds, *Chem. Rev.*, 2010, **110**, 268–320.
27 K.-R. Lee and G. A. Sotzing, *Chem. Commun.*, 2013, **49**, 5192–5194.
28 P. Chandrasekhar, B. J. Zay, C. Cai, Y. Chai and D. Lawrence, *J. Appl. Polym. Sci.*, 2014, **131**, 41043.
29 R. H. Bulloch, J. A. Kerszulis, A. L. Dyer and J. R. Reynolds, *ACS Appl. Mater. Interfaces*, 2014, **6**, 6623–6630.
30 X. Yu, M. Chang, W. Chen, D. Liang, X. Lu and G. Zhou, *ACS Appl. Mater. Interfaces*, 2020, **12**, 39505–39514.
31 Y. Zhu, M. T. Otley, A. Kumar, M. Li, X. Zhang, C. Asemota and G. A. Sotzing, *Chem. Commun.*, 2014, **50**, 8167–8170.
32 M. Li, O. A. Yassin, M. L. Baczkowski, X. Zhang, R. Daniels, A. A. Deshmukh, Y. Zhu, M. T. Otley and G. A. Sotzing, *Org. Electron.*, 2020, **84**, 105748.
33 J. Jensen, M. Hösel, A. L. Dyer and F. C. Krebs, *Adv. Funct. Mater.*, 2015, **25**, 2073–2090.
34 M. Schott, L. Niklaus, C. Müller, B. Bozkaya and G. A. Giffin, *Mater. Adv.*, 2021, **2**, 4659–4666.
35 P. Andersson Ersman, U. Boda, I. Petsagkourakis, J. Åhlin, U. Posset, M. Schott and R. Brooke, *Adv. Eng. Mater.*, 2023, **25**, 2201299.
36 A. L. Dyer, M. R. Craig, J. E. Babiarz, K. Kiyak and J. R. Reynolds, *Macromolecules*, 2010, **43**, 4460–4467.
37 X. Chen, Z. Xu, S. Mi, J. Zheng and C. Xu, *New J. Chem.*, 2015, **39**, 5389–5394.
38 G. Atakan and G. Gunbas, *RSC Adv.*, 2016, **6**, 25620–25623.
39 Z. Xu, X. Chen, S. Mi, J. Zheng and C. Xu, *Org. Electron.*, 2015, **26**, 129–136.
40 C. Lin, T. Endo, M. Takase, M. Iyoda and T. Nishinaga, *J. Am. Chem. Soc.*, 2011, **133**, 11339–11350.
41 S. Rajappa and A. R. Deshmukh, in *Comprehensive heterocyclic chemistry III*, ed. A. R. Katritzky, Elsevier, Amsterdam, 2009, vol. 4, pp. 741–841.
42 M. A. Ochieng, J. F. Ponder and J. R. Reynolds, *Polym. Chem.*, 2020, **11**, 2173–2181.
43 A. J. Heeger, R. Pethig, R. J. Gillespie and P. Day, *Philos. Trans. R. Soc., A*, 1985, **314**, 17–35.
44 Deutsches Institut für Normung, e.V. DIN 5033-1:2017-10, *Colorimetry – Part 1: Basic terms of colorimetry*, Beuth Verlag, Berlin, 2017.
45 T. Dumas, D. Guillaumont, P. Moisy, D. K. Shuh, T. Tyliszczak, P. L. Solari and C. D. Auwer, *Chem. Commun.*, 2018, **54**, 12206–12209.
46 U. Posset, B. Herbig, G. Schottner, K. Zaghib, J.-F. Labrecque, A. Guerfi, M. Perrier, R. Ruffo, M. Salamone, C. Mari, L. Beverina and G. Pagani, *EU Pat.*, 2570846A1, 2011.

